PCCP

PAPER

View Article Online
View Journal | View Issue

Cite this: *Phys. Chem. Chem. Phys.*, 2018, **20**, 6657

An experimental and theoretical investigation of XPS and NEXAFS of 5-halouracils†

M. C. Castrovilli, [a] P. Bolognesi, [a] E. Bodo, [b] G. Mattioli, [a] A. Cartoni[b] and L. Avaldi *[a]

Received 2nd January 2018,
Accepted 31st January 2018

DOI: 10.1039/c8cp00026c

rsc.li/pccp

The C, N and O 1s excitation and ionization processes of 5X-uracil (X = F, Cl, Br, and I) were investigated using near edge X-ray absorption fine structure (NEXAFS) and X-ray photoemission (XPS) spectroscopies. This study aims at the fine assessment of the effects of the functionalization of uracil molecules by halogen atoms having different electronegativity and bound to the same molecular site. Two DFT-based approaches, which rely on different paradigms, have been used to simulate the experimental spectra and to assign the corresponding features. The analysis of the screening of the core holes of the different atoms *via* electronic charge density plots has turned out to be a useful tool to illustrate the competition between the partially aromatic and partially conjugate properties of this class of molecules.

1. Introduction

Core electrons in a molecule are essentially localized on specific atomic sites and their excitation and binding energies are very sensitive to changes in the chemical environment. In particular, when a molecule contains several, chemically nonequivalent atoms of the same species, the chemical shift of the corresponding core levels provides information on molecular properties,[1] such as proton affinity,[2] chemical equilibrium and reactivity parameters.[3] In this regard, the measurement of inner-shell excitation and ionization energies provides an effective local probe of the chemical environment of the atoms in the molecule and makes it possible to establish ''site-dependent'' structure-properties relationships in a variety of chemical compounds.

The physics and chemistry of small biological molecules offer an exceptionally significant benchmark for core spectroscopies. Such systems are relevant for several fields, from biomedicine and biotechnologies to astrochemistry and astrobiology as well as for the realization of sensors and heterogeneous materials. Recently, a number of inner shell studies of biomolecules and their precursors have been reported.[4–10] These works proved that XPS and NEXAFS spectroscopies can provide accurate information on the electronic structure, partial atomic charge and electronegativity of biomolecules and are able to discriminate between different molecular conformations in space.

We have performed a gas-phase investigation of the electronic structure of the series of 5-halosubstituted uracils, probing them with synchrotron radiation using core-level absorption and emission measurements. Our interest is motivated by the fact that uracil, cytosine and thymine are the three nucleic acids based on the pyrimidine structure and are the building blocks of DNA and RNA. Moreover, halouracils have found applications as radiosensitisers in radiotherapy. For example, it was discovered more than 40 years ago that 5-bromodeoxyuridine (an analogue of thymidine) can be embodied in the DNA by replacing thymidine enhancing radiotherapeutic effects, most likely *via* the cascade Auger emission induced by the decay of the ionized halogen atom.[11,12] Finally, uracil can be considered as a conjugated molecule having a partial aromatic character,[13] thus offering an interesting opportunity of comparison between the fundamental properties of Hückel-compliant precursors such as halopyrimidine[14] and the present halouracil.

We have recently devoted some attention to pyrimidine and its halogenated compounds[14–18] studying the effect of the specific halogen atom substitution and site of the halogenation in valence and core photoemission, photoabsorption and photofragmentation. In the present work, we increase the complexity of targets and present new results of a NEXAFS and XPS investigation of the C, N and O 1s states in the series of 5-halouracils. The experimental results are compared with those obtained using different theoretical approaches, all based on (time dependent) density functional theory (DFT).[19] Theoretical spectroscopic methods and their reliability have advanced noticeably in the last decade and it is now possible to calculate the spectroscopic properties of complex molecular systems and predict their chemical and physical behavior with a great accuracy.[20] In particular the spectroscopy of free molecules in the gas-phase represents an ideal playground

[a] *Istituto di Struttura della Materia-CNR, ISM-CNR, Area della Ricerca di Roma 1, CP10, 00015 Monterotondo Scalo, Italy. E-mail: lorenzo.avaldi@ism.cnr.it*
[b] *Dipartimento di Chimica, Sapienza Università di Roma, Pl.e Aldo Moro 5, 00185, Roma, Italy*

† Electronic supplementary information (ESI) available. See DOI: 10.1039/c8cp00026c

for ab-initio calculations because they can easily provide information on the properties of a system in the absence of environmental effects. We will show that two DFT-based approaches built on different paradigms are able to fully describe the energy of the core electrons and to assign the experimental spectra, also offering an unmatched point of view on the screening pattern induced in such peculiar π-conjugate molecules by the formation of core holes.

2. Experimental

The NEXAFS and XPS spectra were recorded at the Gas Phase Photoemission beamline of the Elettra synchrotron radiation source.[21] The light source is an undulator of period 12.5 cm, 4.5 m long. The 100% linearly polarised radiation from the undulator is deflected to the variable-angle-spherical grating monochromator[22] by a prefocusing mirror. The monochromator, placed between entrance and exit slits for photon beam resolution, consists of two optical elements: a plane mirror and a spherical grating. Five interchangeable gratings cover the energy region 13–1000 eV, with a typical resolving power of about 10 000. Two refocusing mirrors after the exit slit provide a circular focus (radius about 300 μm) at the interaction region in the experimental chamber.

The NEXAFS spectra have been collected using a channeltron multiplier close to the interaction region to detect the ions produced by the decay of the excited molecular states. The ion detector has been placed at the pseudo 'magic angle', 54.7° with respect to the photon beam polarization axis and 35.3° with respect to the photon propagation direction, so that the measured cross section is not affected by the asymmetry parameter β. The electron analyzer used for the XPS spectra[4] is placed at the magic angle in the parallel plane, *i.e.* in the plane defined by the electric vector of the light and the photon propagation direction. In this geometry, the measurements of the photoelectron spectrum are insensitive to the variation of the asymmetry parameter β.

All samples were purchased from Sigma-Aldrich, with purity higher than 95% and used without further purification. At room temperature, they are powders and a furnace was used for their evaporation. The evaporation temperatures (from 432 K for 5F-uracil to 473 K for 5I-uracil) were determined before the experiment to avoid thermal decomposition.

In the NEXAFS measurements the photon energy scale was calibrated using a mixture of the molecule under study and a calibration gas with well known absorption peaks in the same energy range, *i.e.* the (C 1s → π*) and (O 1s → π*) transitions of CO_2 at 290.77 eV[23] and 535.4 eV,[24] respectively, and (N 1s → π*) of N_2 at 401.87 eV.[25] The energy resolution was approximately 70 meV in the C 1s spectra and 100 meV in the N and O 1s spectra. The NEXAFS spectra have been obtained by scanning the photon energy over the range of interest and acquiring the ion signal. The spectra were then normalized to the simultaneously recorded photon beam intensity. The normalization procedure was particularly critical near the carbon K edge, where carbon contamination of the beamline optics results in rapidly varying transmission of the radiation. The average acquisition time necessary to reach the present level of accuracy was of the order of a few seconds/point, depending on the sample.

The C, N and O 1s XPS spectra were recorded at about 100 eV above their respective ionization thresholds, using an energy resolution of about 300 meV. A kinetic energy of about 100 eV in the photoelectron spectra guarantees that PCI effects[26] can be neglected in the data analysis. The energy spectra were calibrated using a mixture of the molecule under study and a calibration gas with well known XPS peaks in the same binding energy range, *i.e.* CO_2(C 1s, v = 0) at 297.69 eV[27] for 5Cl-, 5Br- and 5I-uracils and CH_4(C 1s, v = 0)[28] at 290.69 eV for 5F-uracil, N_2 (N 1s)[29] at 409.9 eV, and CO_2 (O 1s)[30] at 541.25 eV. We did not calibrate the transmission of the analyzer, but it is expected to be constant over the narrow energy ranges of the core level spectra.

3. Computational details

The theoretical values of vertical XPS ionization energy, IE, have been calculated in both ketonic and enolic forms of the substituted uracils using two different computational frameworks, both based on density functional theory (DFT).

In the former case the *ab initio* simulations have been performed using a plane-wave/pseudopotential/supercell approach, as implemented in the Quantum-ESPRESSO package.[31] The equilibrium geometries have been found by fully relaxing all the molecules accommodated in large cubic supercells (25 Å^3) to minimize the occurrence of spurious interactions between periodically replicated images. Total energies have been calculated using norm-conserving Troullier–Martins atomic pseudopotentials,[32] a plane-wave basis set, and the B3LYP hybrid exchange–correlation functional.[33,34] A further Makov–Payne correction has been also applied to energy values in order to correct the spurious electrostatic interactions between periodically replicated images of the molecules. Satisfactorily converged results have been achieved by using cutoffs of 90 Ry on the plane waves and of 360 Ry on the electronic density, respectively, as well as the Gamma point for the *k*-point sampling of the Brillouin zone. H(1s), C(2s) and (2p), N(2s) and (2p), O(2s) and (2p) electrons as well as the ones of the *n*s and *n*p outer shells of all the halogen atoms have been treated as valence electrons. All of the inner shell electrons are embedded in the pseudopotentials. XPS chemical shifts have been estimated by total energy differences between "standard" and "core-hole" calculations.[14,35–37] In the latter case, an excited state pseudopotential containing a 1s core hole has been used in place of the regular pseudopotential. A different calculation has been performed for each nonequivalent atom. The energy differences between the standard and core-hole calculations have been compared with the corresponding difference obtained for the C or O (N) atom of a CO_2 (N_2) molecule, accommodated in the same supercell and used as a reference for both the calculated and experimental chemical shifts. In the following the results obtained with this method will be labeled QE.

In the latter case the ground state geometry of the neutral molecules has been obtained by a standard optimization procedure

performed with the ORCA code[38] at the all-electron B3LYP[33] level using the ZORA-def2-TZVP(-f)[39] basis set and accounting for relativistic scalar effects using the ZORA approximation.[40]

Core electron IEs have been calculated using the ΔSCF approach at the previously computed geometries by means of the ADF[41] suite of programs. The energy of the singlet ground state molecules was computed using an all electron calculation with the pw86x-pw91c[42] functional with the Slater type basis set QZ4P[43] and adopting the RA-X2C approach[44] for relativistic effects. The energy of the core-ionized doublet ion was computed within the same approach and creating a localized hole in the proper 1s orbital. The IE was then computed using the formula:

$$\mathrm{IE} = E_{\mathrm{KS}}(\mathrm{M}^{+}) - E_{\mathrm{KS}}(\mathrm{M}) \quad (1)$$

where $E_{\mathrm{KS}}(\mathrm{M}^{+})$ and $E_{\mathrm{KS}}(\mathrm{M})$ are the bonding energy of the ion and of the neutral, respectively. The final IE values have not been corrected by scaling or shifted. In the following the results obtained with this method will be labeled ADF.

The NEXAFS spectra have been computed only for the ketonic forms of the substituted uracil molecules using the optimal geometries at the B3LYP/ZORA-def2-TZVP(-f) level obtained as previously illustrated. The NEXAFS spectra were computed with the ORCA[38] code using an all-electron approach (with the ZORA scheme for scalar relativistic effects) and the minimally augmented relativistic re-contraction of the def2-QZVPP basis set.[45] The NEXAFS spectra, in particular, were simulated by computing the first 100 excited states in the TD-DFT approximation by limiting the hole creation space to the range of core orbitals of each element.

The theoretical spectra have been obtained by convoluting the stick spectra with a Gaussian line-shape of width 0.5 eV and height equal to the absolute absorption. Several tests on the performance of different functionals have been performed (see Tables S7 and S8 in section ESI 2.4†). Consistent with previous literature[46–48] the best results have been obtained either using the CAM-B3LYP[49] or the B2PLYP[50] functionals. For brevity, in the following we shall report only the CAM-B3LYP results. The calculated DFT excitation energies have been shifted to match the lowest energy experimental spectral feature. The shift depends on the element (C, N or O), but we kept it constant throughout the halogen variation. The mismatch between the DFT and the measured transition energies in the core excitation spectra depends mainly on the percentage of exact exchange in the DFT functional. B3LYP has a relatively small fraction of exact exchange and the correction turns out to be around 10–12 eV. Functional rich in exact exchange as the B2PLYP (50%) requires a much smaller shift of only a few hundreds of meV.[51] The mismatch is practically systematic in a homologue series of molecules and does not alter significantly the relative energies or the spectral shapes.

4. Results

4.1 XPS

We measured the XPS spectra of all the 5-halouracils at the C, N and O K-edges. For the sake of shortness (compactness) only the XPS spectra of 5F-uracil are shown in Fig. 1. Once the energy scale is calibrated *versus* the benchmark lines (see the Experimental section) the deconvolution of the different components has been achieved by a fit with a series of Gaussian functions.

The C 1s spectrum is composed of three peaks, the one at lower ionization energy being broader than the other two. The different widths and intensities of the peaks reflect the Franck–Condon factors for each core level ionization process. These three peaks are related to the ionization of the four non-equivalent carbon atoms in the molecule. According to the previous results in uracil,[52] increasing IEs for the C5, C6, C4 and C2 atoms, respectively, have been measured. Therefore, the peak at higher IE can be associated with the C2 atom, located between the two NH groups and suffering from the depletion of electronic density due to charge transfer to the O atom. Similarly due to the presence of only one NH group, the peak due to the ionization of the C4 atom is expected to appear at lower IE. Thus the second peak in the spectrum is attributed to the ionization of the C4 atom. Finally, the broader structure is assigned to the ionization of the C5 and C6 atoms. The order of the two can be established only *via* the information provided by the calculations. A sound assignment of the peak at the lowest IE along the whole series requires therefore additional information from DFT simulations. In the case of the O and N atoms the XPS spectra display only one peak, which receives contributions from the N1 and N3 and O7 and O8 atoms, respectively. Accordingly in the fit the width and area of the two components have been constrained to be equal. The energy difference between the two components of each peak can be attributed to both initial-state chemical and final-state screening effects.[52]

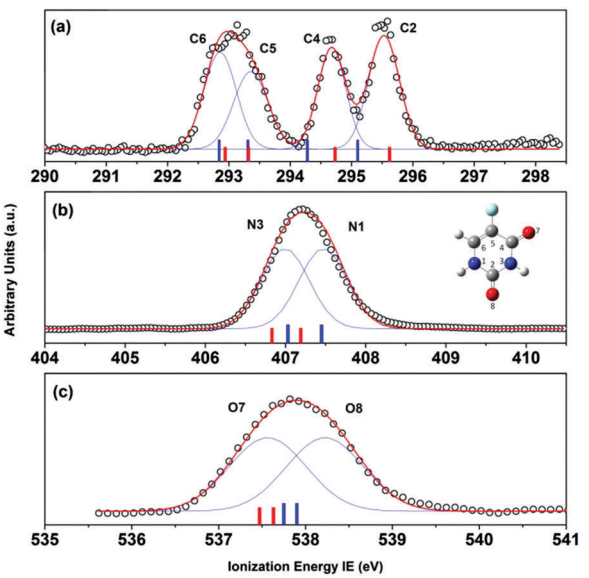

Fig. 1 The C (a), N (b) and O (c) XPS spectra of 5F-uracil. The red and blue full lines represent the fit and the different contributions to the measured spectra. The red and blue bars are the theoretical predictions obtained using the DFT QE and ADF calculations, respectively. In the middle panel a scheme of the 5F-uracil with the numbering of the different atoms is reported.

As for nitrogen, a higher screening contribution of the two neighboring, electron-rich C═O groups in the case of N3 suggests a corresponding IE lower than the N1 one. Less can be inferred in the case of O atoms on the grounds of simple considerations on the chemical properties of neighboring atoms and groups. A final assignment of N and O components can be provided only through the comparison of measurements and calculations, as in the case of the C5 and C6 components of the C spectra.

As an additional degree of freedom that characterizes such a kind of system, it is known that nucleic acids may exist as tautomers, and it was observed that at the temperature of a few hundreds Kelvin in gas phase experiments tautomers of guanine and cytosine are significantly populated.[53] However this is not the case of thymine, adenine, and uracil, which exist in the single keto-form,[54] as also proved by the present work where the calculations for the different eno-forms (reported in the section ESI.1†) do not match the experimental measurements. All the measured values are collected in Table 1, where they are compared with the predictions of the DFT QE and ADF theoretical approaches. For the sake of completeness also the measured and calculated values for the un-substituted uracil molecule by Feyer *et al.*[52] have been reported in the same table.

4.2 NEXAFS

We measured the NEXAFS spectra of all the 5-halouracils at the C, N and O K-edges from the energy just below the 1s → LUMO up to several eV above their respective ionization threshold. As for XPS, also in the case of NEXAFS the 5F-uracil absorption spectra at the three edges have been used as examples and are shown in Fig. 2. The full set of NEXAFS spectra will be shown together with the theoretical predictions in the next section and the energies of the main features observed are collected in Table 2. Although a detailed assignment of the features observed in the spectra of Fig. 2 can be achieved only with the support of

Table 1 Measured and calculated values of the IE of the different atoms in uracil and 5X-uracil (X = F, Cl, Br, and I). The experimental and theoretical data for uracil, labeled by "*", are taken from ref. 52. In brackets the experimental uncertainty in eV

	Expt. (eV)		ADF (eV)	ΔE (ADF,expt) (eV)	QE (eV)	ΔE (QE,exp) (eV)
Uracil (ref. 47)	537.6*	O7	537.41*			
		O8	537.70*			
	406.8*	N1	406.92*			
		N3	406.50*			
	292.8*	C6	292.78*			
	295.4*	C2	295.54*			
	294.4*	C4	294.41*			
	291.0*	C5	290.86*			
5F-uracil	537.56 (0.26)	O7	537.75	0.19	537.47	−0.09
	538.22 (0.26)	O8	537.90	−0.32	537.63	−0.59
	407.47 (0.05)	N1	407.46	−0.01	407.19	−0.28
	406.99 (0.05)	N3	407.03	0.04	406.83	−0.16
	293.00 (0.04)	C6	292.84	−0.16	292.94	−0.06
	295.68 (0.04)	C2	295.10	−0.58	295.62	−0.06
	294.83 (0.04)	C4	294.28	−0.65	294.73	−0.10
	293.51 (0.04)	C5	293.31	−0.20	293.32	−0.19
5Cl-uracil	537.28 (0.09)	O7	537.67	0.39	537.39	0.11
	537.79 (0.07)	O8	537.86	0.07	537.61	−0.18
	406.88 (0.07)	N1	407.36	0.48	407.11	0.23
	406.63 (0.07)	N3	406.96	0.33	406.76	0.13
	292.68 (0.04)	C6	292.70	0.02	292.86	0.18
	295.42 (0.04)	C2	295.01	−0.41	295.58	0.16
	294.53 (0.04)	C4	294.17	−0.36	294.65	0.12
	292.12 (0.04)	C5	292.27	0.15	292.28	0.16
5Br-uracil	537.17 (0.09)	O7	537.62	0.45	537.36	0.19
	537.74 (0.09)	O8	537.82	0.08	537.59	−0.15
	406.95 (0.19)	N1	407.30	0.35	407.05	0.10
	406.45 (0.13)	N3	406.90	0.45	406.71	0.26
	292.78 (0.15)	C6	292.62	−0.16	292.83	−0.05
	295.54 (0.15)	C2	294.94	−0.60	295.57	0.03
	294.63 (0.15)	C4	294.11	−0.52	294.64	0.01
	291.93 (0.15)	C5	291.91	−0.02	291.95	0.02
5I-uracil	536.82 (0.07)	O7	537.55	0.73	537.30	0.48
	537.43 (0.08)	O8	537.76	0.33	537.55	0.12
	406.53 (0.11)	N1	407.21	0.68	406.96	0.43
	405.98 (0.09)	N3	406.83	0.85	406.64	0.66
	292.51 (0.04)	C6	292.49	−0.02	292.75	0.24
	295.24 (0.04)	C2	294.84	−0.40	295.55	0.31
	294.30 (0.04)	C4	294.00	−0.30	294.59	0.29
	291.22 (0.04)	C5	291.45	0.23	291.51	0.29

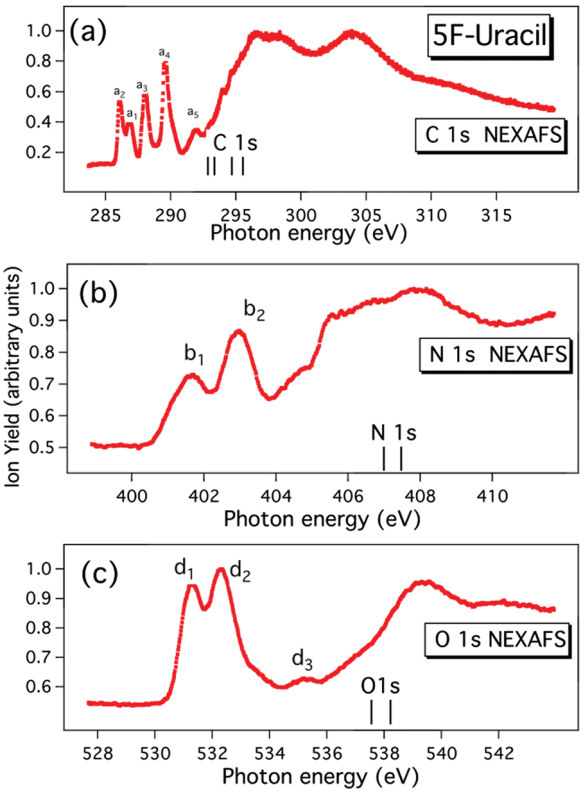

Fig. 2 The experimental C (a), N (b) and O (c) 1s absorption spectra of 5F-uracil. The vertical bars indicate the experimental IEs of the non-equivalent atoms measured in this work.

calculation, some general observations can already be anticipated here. All the spectra display intense peaks in the lowest energy part, *i.e.* four for the C 1s spectrum and two in the case of N 1s and O 1s spectra. These strong bands can be mainly associated with the transition to the LUMO from the non-equivalent atoms of the molecule. The order depends on the respective chemical shifts, which in turn depends on the local environment.

It is interesting to observe that at variance with the XPS spectra, where a single peak for the two chemically distinct atoms is observed, the NEXAFS spectra at O and N edges show two well resolved resonances. Approaching the inner shell IE, the higher energy part of the absorption spectra displays other bands, which can be attributed either to transitions to other valence states and/or to Rydberg levels. It is likely that in the case of N 1s the presence of several transitions with similar oscillator strengths enhances and broadens the structures in the region 2–3 eV below the IEs. A similar situation has been observed by Feyer *et al.*[55] in uracil. The measurement at the C 1s edge extends for more than 10 eV above the IEs. This allows the identification of two shape resonances at about 298 and 303 eV, respectively.

5. Discussion

The trend of the IE of the different 1s orbitals in C, N and O *versus* halogenation is well summarized by the correlation diagrams, which are reported in Fig. 3 together with the experimental values of uracil.[52] Such a trend, which depends on the different screening of the core hole, can be partially understood considering the inductive and resonance models used to explain a variety of chemical properties, such as the reactivity in electrophilic aromatic substitutions[56] of large families of substituents in aromatic compounds and successfully adopted for the interpretation of the XPS spectra of halopyrimidines[14] and nitrotoluenes.[36] In the case of halouracils, the change of the chemical environment due to the electronegativity of the halogen atoms has a strong inductive effect on the nearest atom to the substituent. This electrostatic effect, being isotropic and depending on the distance, affects, although

Table 2 Experimental values of the features observed in the NEXAFS spectra of the uracil and halogenated 5X-uracil (X = F, Cl, Br, I). (*) The experimental data for uracil are from ref. 55

C 1s	a_1	a_2	a_3	a_4	a_5	Shape resonance	Shape resonance
Uracil*	284.79 (C_5)	286.11 (C_6) 287.78	288.00 (C_4)	289.50 (C_2) 290.24			
5F-uracil	286.64	286.07	287.98	289.51	292.01 293.96	298.26	303.94
5Cl-uracil		285.95	287.94	289.35 290.26 (shoulder)	291.98	297.51	303.38
5Br-uracil		285.98	287.93	289.42		297.53	303.38
5I-uracil	285.31	286.01	287.93	289.42		296.41	303.15
N 1s	b_1	b_2	b_3			Shape resonance	
Uracil*	401.4	402.62	404.1 ($1\ s^{-1}$ 4s/4p) 405.8				
5F-uracil	401.7	402.98				407.98	
5Cl-uracil	401.7	402.98	404.58			407.68	
5Br-uracil	401.34	402.86	404.45			407.39	
5I-uracil	401.32	403.07	404.51			407.65	
O 1s	d_1	d_2	d_3			Shape resonance	
Uracil*	531.37	532.35	535.38				
5F-uracil	531.27	532.35	535.25			542.34	
5Cl-uracil	531.4	532.77	536			541.08	
5Br-uracil	531.33	532.18	535.43			541.08	
5I-uracil	531.16	532.03	535.22			540.11	

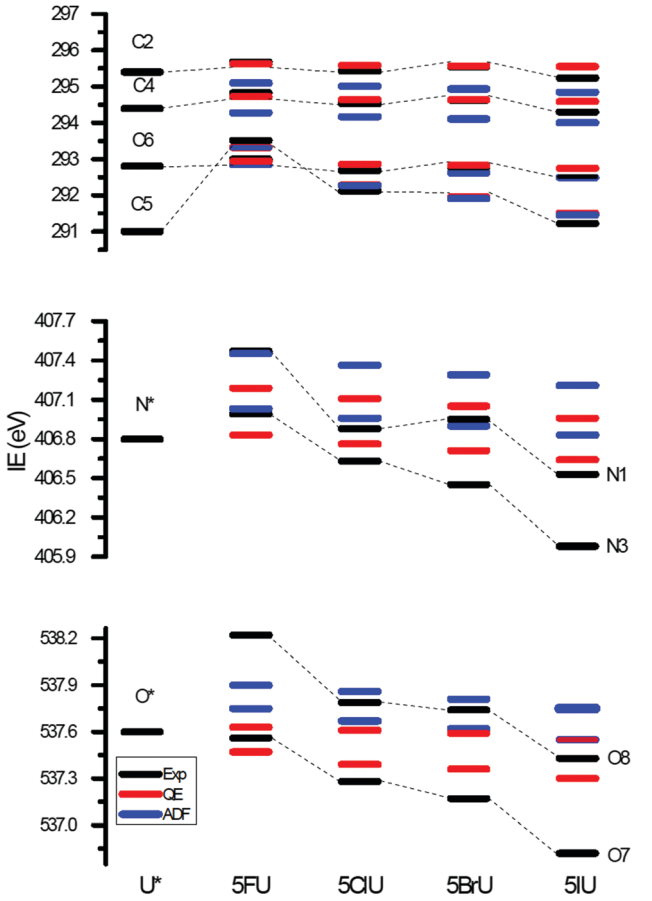

Fig. 3 Correlation diagram of the four nonequivalent C, two nonequivalent N and two nonequivalent O atoms of the 5X-uracil molecules. The experimental IEs from Table 1 (black dotted lines) are compared with the ADF (blue lines) and QE (red line) calculations. The experimental data of uracil are from ref. 52, where only the centroid of the N and O peaks has been reported.[52]

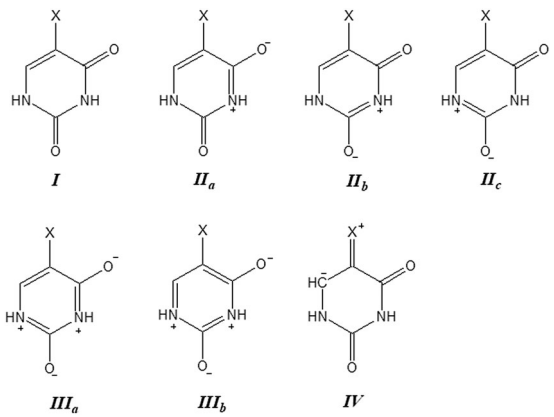

Fig. 4 Resonance structures of 5X-uracil molecules.

in minor way, also the IEs of the other atoms of the molecule. The resonance effect on the other hand assumes that a resonance structure exists (see structure IV in Fig. 4) where the halogen atom carries a positive charge and forms a double bond with its C neighbor, while the ring acquires an electron. This additional negative charge is preferentially localized in the ortho and para positions with respect to the halogen through the fully aromatic resonance structures IIIa,b (Fig. 4).

However, the only partial aromatic character of uracil and of its derivatives can be responsible for peculiar deviations from the simple models mentioned above. Therefore, before discussing the effect of halogenation on IEs, we preliminarily assess the conjugate or aromatic character of uracil derivatives by discussing the results of simulations involving the core-ionization of C, N and O in the case of 5Br-uracil, taken as a representative example.

In detail, Fig. 5 shows difference-density plots obtained by subtracting the site-specific charge density of core-ionized molecules to the charge density of the neutral system. Such plots quantify the displacement of the valence electronic charge density from blue zones to red zones of the molecule in order to screen the different kinds of 1s core hole. Indeed, anisotropic screening patterns of core holes related to the resonance structures displayed in Fig. 4 shed light on the action of inductive and resonant mechanisms as well as on the aromatic *versus* conjugate properties of the molecules.

In this regard, some specific connections deserve an insightful discussion. In the case of C2, we note that an almost spherical red region, partly distorted by the triangular symmetry of the site, represents the charge accumulation screening the C 1s core hole. The three blue arrows indicate regions where an isotropic charge depletion corresponds to the inductive contribution to such screening. Small in-plane rearrangements of the charge density along the sigma skeleton of the molecule are present, which have also been reported in the case of halogenated pyrimidines as well as in nitrotoluene isomers as discussed in previous works.[14,36] More interestingly, no π-type (out of plane) displacement can be observed in the case of the two N atoms holding an *ortho* position with respect to C2. This is clearly understood by observing the two fully-aromatic resonance structures of the molecule (IIIa and IIIb in Fig. 4), in which both N atoms carry a positive charge and cannot, therefore, delocalize excess density on the neighboring C2 site. In contrast, no similar mechanism hinders the aromatic screening of the C2 core hole clearly visible on the C5 site (green arrow), thus confirming the partial aromatic character of the molecule. A conjugation mechanism must be invoked instead in the case of the screening of the C2 core hole from O7 (magenta arrow) through the resonance structure IIc, given the impossible transposition of the excess O charge through the aromatic resonance structures IIIa and IIIb. Finally, Br also participates in the screening of the C2 core hole through the resonance structure IV, with the excess charge resonating in the C2 position due to the partial aromatic character of the molecule. However, the Br contribution cannot be appreciated in Fig. 5 due to its more diffuse nature than that corresponding to the smaller C, N and O atoms. A density plot obtained by using a smaller value for the isosurface sampling (0.003 e a.u.$^{-3}$ instead of 0.007 e a.u.$^{-3}$) has been provided in Fig. ESI.1 of the section ESI.3†. Rather than discussing similar resonant mechanisms working in the case of the screening of different core holes and all evidenced by green arrows in Fig. 5,

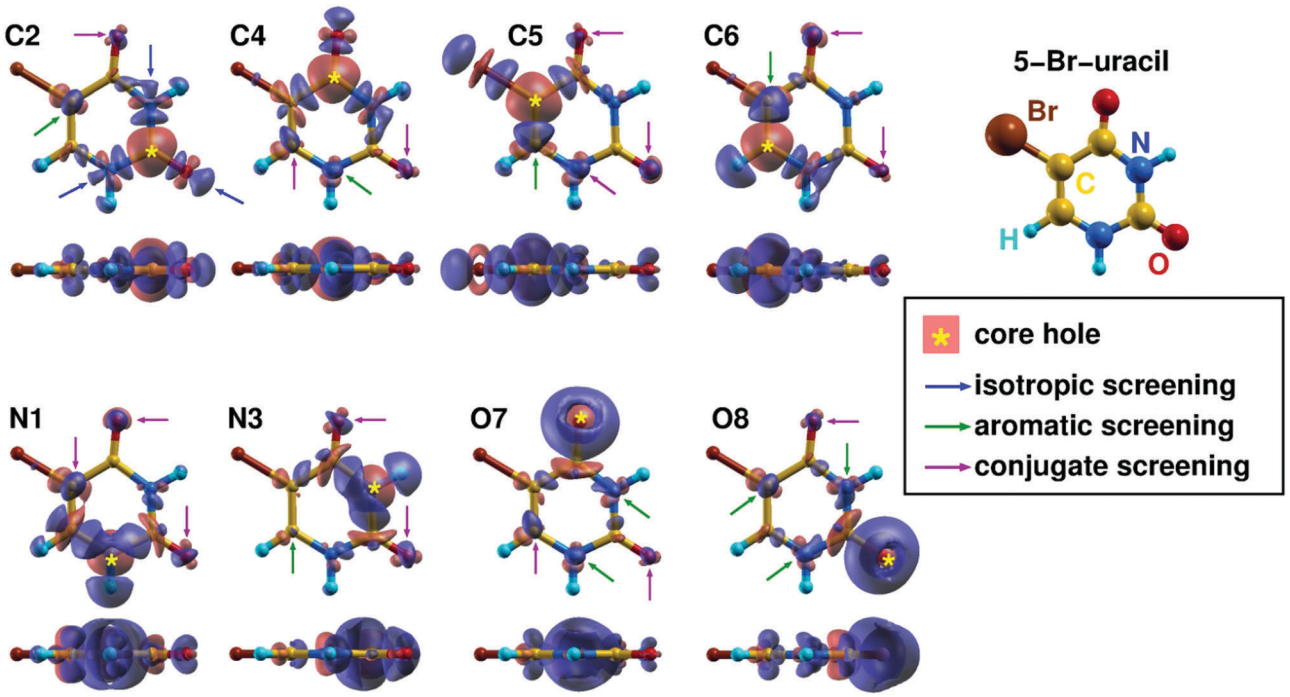

Fig. 5 Difference density maps (top and side view) of "standard" *versus* "core hole" calculations (see the text). Blue and red zones represent positive and negative isosurfaces of electronic density sampled at 0.007 electrons per a.u. Blue, green and magenta arrows indicate isotropic, aromatic and conjugate mechanisms, respectively, acting in the screening of the different core holes, as detailed in the text.

we finally focus on strongly antiaromatic mechanisms, corresponding to π-type screening coming from *meta* positions with respect to the core hole, never observed in the case of the previously investigated halopyrimidines.[14] Such contributions are indicated by the magenta arrows in Fig. 5. This is the case of the C4, C5 and N1 core holes, respectively, screened by π-type contributions coming from the C6, N1 and C5 positions. This behavior is due to the special character of the C5═C6 double bond, which is the only double bond present in the uracil ring in the regular structure I and also the most represented in other resonance structures shown in Fig. 4. All the *meta* screening patterns active on the uracil ring involve in fact the transposition of such a bond. Such an easy transposition is also evidenced by the very strong π-type contribution of the C6 (C5) position to the screening of the C5 (C6) core hole, in further agreement with a minority contribution of the fully aromatic resonance structures to the properties of halouracils.

After this preliminary analysis, we can focus on the effect of halogenation with different species on the IEs of C, N and O atoms. The observed large XPS shift in the IE of the C5 atom, the one directly involved in the bond with the halogen, is attributed to the inductive effect. Moving from 5F- to 5I-uracil the decreasing value of the electronegativity of the halogen atoms makes the IEs decrease in absolute value, reducing the shift with respect to the non halogenated molecule from 2.0 to 0.2 eV. In the case of 5F-uracil the strong inductive effect on C5 results in a variation in the order of the IEs of the four non-equivalent C atoms, with a swap between IE(C6) and IE(C5) with respect to uracil. The order of the IEs is restored to the one of the unsubstituted molecule, IE(C2) > IE(C4) > IE(C6)> IE(C5), already in the case of 5Cl-uracil. C4 suffers by the combined effect due to the O and halogen atoms, and its peak in 5F-uracil displays a shift of about 400 meV with respect to uracil. In 5Br-uracil, IE has no appreciable changes with respect to 5Cl-uracil. This might be partially explained by the small variation of the electronegativity going from Cl to Br. Indeed this variation is the smallest along the series considered here. The other contribution to the observed IEs, *i.e.* the resonance effect, should work against the one due to the inductive effect and reduce the IE.

In the case of the N atoms the calculated IEs of the N1 atom are always higher than the N3 ones. This is generally due to the charge displacement from the two neighboring electron-rich C═O groups, which provide a better screening of the core hole in N3 through the resonance structures IIa and IIb with respect to N1, which can only benefit from the conjugation with O8 through the resonance structure IIc. Regarding the effect of halogens, we note that the centroid of the N 1s feature in 5F-uracil is around 0.5 eV higher than in uracil. Such a strong inductive effect of fluorine is not mitigated by resonant structures that allow the participation of its electrons in the screening of the N core hole. The blue shift with respect to the corresponding uracil line is therefore more pronounced than that discussed above in the case of the C4 and C6 positions, even if these two C atoms are nearer to F than the two N atoms. This difference already vanishes in the case of 5Cl- and 5Br-uracils and a red shift of about 300 meV is observed in 5I-uracil.

A similar situation is observed in the case of the ionization of the O atoms, where the IE of the O8 atom is always higher than that of the O7 one. Such a difference is not due to an effect

of the halogen atom because it is almost constant along the whole series. Fig. 5 suggests that the core hole in O8 is screened through a regular aromatic-like resonance pattern by π-type contributions coming from both N atoms (*ortho* positions with respect to the =O substituent) and from the C5 position (*para*). The special antiaromatic mechanism discussed above is involved instead in the case of O7, with a π-type contribution to the screening coming from the C6 position through the transposition of the C5=C6 bond. This is a further suggestion of the minority aromatic character of uracil and of its halogenated derivatives.

As far as the comparison with theory is concerned, a general agreement between the predicted values and experimental values exists. The ADF results appear to underestimate the IEs in the case of the carbon atoms with a maximum displacement of about 600 meV for C2 in 5Br-uracil. Considering that the IEs in the ADF method are obtained on the absolute scale, these results are quite remarkable. The QE results, calibrated *versus* the experimental IEs of the CO_2 molecule, tend to overestimate the carbon IEs and in general their displacement from the experimental values is in average about 200 meV. The situation reverses in the case of N and O IEs where the ADF results overestimate and the QE results underestimate the experiments. In the case of N and O atoms it can also be observed that while both series of simulations predicts a decreasing energy for the peaks going from F to I, the theoretical shift is definitely smaller than the experimental one. Moreover in both cases the experimental splitting of the two components appears to be larger, up to a factor of three in the O case, than in theoretical calculations.

Since the first proposal of XPS for chemical analysis[57] a few attempts to correlate the shifts of the binding energy of a core electron with charges assigned to the atoms have been published. These charges were estimated from simple electronegativity considerations or from some kind of molecular orbital calculations. T. D. Thomas[58] in a study of halomethanes concluded that there is a linear correlation between the binding energy shifts and the electronegativity of the ligands. In Fig. 6 the difference between the experimental IEs of different atoms in the halouracil molecules studied here and the corresponding one measured in uracil by Feyer *et al.*[52] are reported *versus* the difference of Pauling electronegativity of the halogen atom and hydrogen. In the case of C5, directly bonded to the halogen, a clear linear dependency is observed (see the red line in Fig. 6). The proportionality constant relating the energy shift to the difference of electronegativity is 1.7 ± 0.2 eV per electronegativity unit, very similar to the one found in the case of halobenzenes,[59] 1.5 eV per electronegativity unit. In the case of the other C atoms (Fig. 6) the linear fit suggests slopes indistinguishable from zero within the fit uncertainty. In the case of the N and O average IEs a linear behaviour can be envisaged with an average slope of 0.61 ± 0.1 eV per electronegativity unit. Such data clearly indicate once more that the strong inductive effect stemming from the substitution of H with a halogen atom dominates the electronic distribution of the nearby atoms, but rapidly decreases further.

As far as the NEXAFS spectra are concerned, the calculations have been extended just above the core IEs to reduce the number of states to be accounted for in the theoretical analysis. Thus, the C, N and O NEXAFS spectra reported in the different panels of Fig. 7 extend up to 294, 410 and 542 eV, respectively.

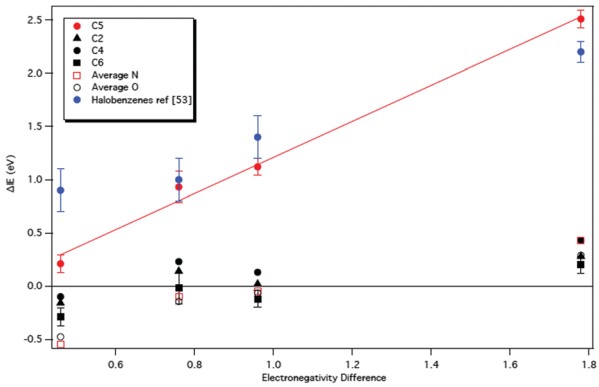

Fig. 6 ΔIE (see the text) *versus* the difference of the electronegativity of the different ligands. C5 (red dots), C2 (black triangle), C4 (black dots) C6 (black squares), average N (red open squares), average O (black open circles). The blue dots are the ΔIEs measured in the case of halobenzenes.[59]

Fig. 7A shows the evolution of the C NEXAFS spectrum along the series of halogenated molecules. In the region between 284–291 eV there are four well resolved main features, labeled a_1–a_4, in 5F- and 5I-uracil that reduce to three in the other two spectra. In the photoabsorption spectrum of uracil[55] the four observed features have been assigned to the Ci 1s → LUMO according to the order i = 5, 6, 4 and 2. We observe in Fig. 7A and Table 2 that three features always occur at the same energy, within the experimental uncertainty, while one moves from 286.64 in 5F-uracil to 285.31 in 5I-uracil, providing a clear fingerprint of the C5 1s → LUMO transitions.

The calculations identify the main sequence of excitations from the four C(1s) cores to the LUMO orbital. The first three at low energy are due to holes in the 1s orbitals of C6, C5 and C4, while the one from C2 is located at higher energy. In 5F-uracil the first two experimental resonances (a_2 and a_1) correspond respectively to the C6(1s) → LUMO and C5(1s) → LUMO excitations. In 5Cl-uracil the C5(1s) → LUMO excitation is shifted towards lower energy and, together with the C6(1s) → LUMO one, gives rise to the first resonance, whose intensity turns out to be larger due to the coalescence of the two bands. In 5Br-uracil and 5I-uracil the C5(1s) → LUMO is progressively shifted at even lower energies. The situation, for Br and I, is complicated by the appearance of a bunch of C5(1s) → LUMO+n mixed excitations in the same region. Such transitions are progressively redshifted through the halogen series (see Table S1, ESI†) and in both cases they are located below the C4 → LUMO transition.

Unfortunately the agreement between the calculated results obtained by using a general-purpose, though accurate, setup (CAM-B3LYP&ZORA-def2-TZVP(-f)) and the experimental spectrum is not preserved at high energies and Rydberg states, which would require asymptotically corrected density functionals and diffuse basis sets. As a result the agreement in such regions of the spectrum is only qualitative. A tentative assignment

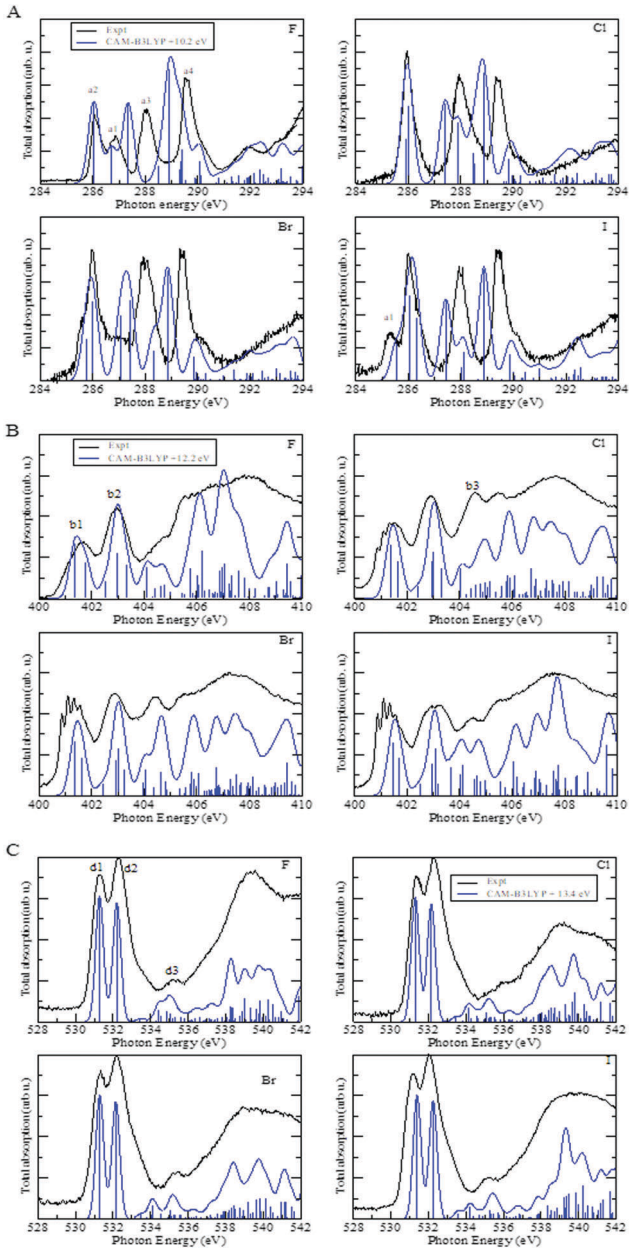

Fig. 7 Calculated and measured absorption spectra of the C (A), N (B) and O (C) K edges for the four 5X-uracil. The CAM-B3LYP results have been shifted by 10.2, 12.2 and 13.4 eV for the C, N and O case, respectively.

however is possible: the resonance at 288 eV can be attributed to the C4 → LUMO excitation in all the four compounds though the theoretical prediction slightly underestimates its energy.

In the N NEXAFS spectra of Fig. 7B, unfortunately a N_2 contamination displaying the typical vibrational band of the N 1s → π_g[60] perturbs the first feature in 5Cl-, 5Br- and 5I-uracil NEXAFS spectra. Considering the oscillator strength and relative energy of the higher excitations in molecular nitrogen[60] we can exclude that other features in Fig. 7B are due to the contamination. The centroid of the first two bands of the spectrum in 5F- and 5Cl-uracil appears at about 300 meV higher energy than in uracil[55] then in 5Br- and 5I-uracil the centroid of the first band is aligned with the same band in uracil, while the second band is blue shifted.

The first band (b_1) is due to the N1 and N3 1s → LUMO excitations. The excitation coming from the N3 atom, located between the two C═O groups, falls at lower energy and it is the most intense of the two. Both transitions are characterized by large oscillator strengths because the LUMO orbital shows an appreciable charge density over both nitrogen atoms (Table S4 in ESI.2.2†). The second band in the spectrum can be considered the sum of at least 4 different excitations. Two of these transitions predicted at about 403.6 and 404.1 eV for the N1 and N3 atoms, respectively, can be attributed to the promotion of the core electrons to very diffuse orbitals with low density. The other two excitations at about 404.1 and 404.5 eV correspond to the promotion of the 1s electron to a π*(A″) orbital (LUMO+1) with an antibonding character over the C–N bonds.

In the experiments the region above 404 eV displays some variations with the halogen. For example the shoulder at about 404.5 eV in 5F-uracil grows in intensity and evolves in a peak in the other halogenated molecules. In uracil similar features have been assigned to N 1s → 4s, 4p Rydberg transitions.[55] The high density of states and the inaccuracy of the present calculations in this region hamper a more detailed assignment of the observed features.

The shape of the absorption spectrum in the region of the O 1s threshold (Fig. 7C) does not display significant changes in the measured series. The energy positions of the features in the different molecules overlap within the experimental uncertainty among themselves as well as with the ones measured in uracil.[55]

The first intense peak is due to the one electron excitation from the 1s orbital of the O7 atom, in the ortho position with respect to the halogen, to the LUMO. The LUMO is a π*(A″) orbital with a high density on the oxygen atom with the electron hole (see Table ESI.6†).

The second peak receives contributions by the one electron excitations from the O8 atom in the *para* position to the halogen. The excited state is a mixed one with contributions from two or three different single excitations: one is O8 1s → π*(A″), delocalized over the relevant C═O bond, while another one involves a more diffuse orbital with an anti-bonding character on the C═O bond.

The third peak has a very low intensity and is due to the O8 1s → LUMO transition. Its low intensity is due to the vanishing overlap between the 1s and LUMO orbitals. This observation is in partial agreement with that reported in ref. 55, where by using the ADC(2) computational method and a relatively small 6-31+G basis set the O8 1s → LUMO transition was considered the main contribution to the second peak in the spectrum.

In Tables ESI-7 and 8† the results of the calculation of the O 1s NEXAFS spectrum using the B2-PLYP functional are also reported. These results are not very different from the ones obtained with the CAM-B3LYP functional. In particular, these calculations confirm that the O8 1s → LUMO transition is characterized by very small oscillator strength and contributes to the third peak in the spectrum at about 535.3 eV.

6. Conclusions

The present joint theoretical and experimental results provide a detailed description of the effects of the halogen substitutions in the inner shell excitation/ionization of the uracil molecule. The ionization energies of the C, N and O 1s electrons in the series of the 5X-uracils (X = F, Cl, Br and I) were measured using XPS. The replacement of H by a halogen mainly results in the withdrawal of the valence charge distribution of the carbon atom, C5, directly linked to the halogen. However, simulations of the core ionization of C, N and O have shown that the screening of the core hole, which determines the value of the IEs, depends on a complex combination of the inductive and resonance mechanisms typical of aromatic compounds as well as on antiaromatic conjugation mechanisms. The latter are due to the only partial aromatic character of uracil and its derivatives. The results show the applicability of the resonance model, proposed in the case of halopyrimdines[14] and nitrotoluenes,[36] also for the description of the properties of partial aromatic molecules like the halouracils. The satisfactory agreement between the measured IEs and the ones predicted using two DFT-based approaches built on different paradigms supports the accuracy reached using such *ab initio* methods in the simulation of the properties of isolated polyatomic molecules.

Among the absorption spectra near the C, N and O K edges, only the C one displays strong effects due to the halogenation. The N and O spectra are substantially independent of halogenation and display almost the same shape in the four investigated molecules. The role of the TD-DFT simulations has been crucial for the assignment of the main structures below the ionization threshold, while due to high density of states the calculations become inaccurate approaching the threshold region.

These results contribute to the fine chemical characterization of uracil derivatives, which are used as building blocks of several biochemical and pharmaceutical compounds. Hence these new results contribute to enrich a useful databank, needed to understand the physical and chemical origin of the photoinduced processes and radiation damage in these biologically relevant molecules.

Conflicts of interest

There are no conflicts to declare.

Acknowledgements

This work was partially supported by the Italian Ministry of Foreign Affairs *via* the Serbia–Italy Joint Research Project "A nanoview of radiation-biomatter interaction".

References

1 S. Svensson, *J. Phys. B: At., Mol. Opt. Phys.*, 2005, **38**, S821.
2 B. E. Mills, R. L. Martin and D. A. Shirley, *J. Am. Chem. Soc.*, 1976, **98**, 2380.
3 B. Lindberg, S. Svensson, P. A. Malmquist, E. Basilier, U. Gelius and K. Siegbahn, *Chem. Phys. Lett.*, 1976, **40**, 175.
4 O. Plekan, V. Feyer, R. Richter, M. Coreno, M. de Simone, K. C. Prince and V. Carravetta, *Chem. Phys. Lett.*, 2007, **442**, 429.
5 O. Plekan, V. Feyer, R. Richter, M. Coreno, M. de Simone, K. C. Prince and V. Carravetta, *J. Phys. Chem. A*, 2007, **111**, 10988.
6 V. Feyer, O. Plekan, R. Richter, M. Coreno, K. C. Prince and V. Carravetta, *J. Phys. Chem. A*, 2008, **112**, 7806.
7 O. Plekan, V. Feyer, R. Richter, M. Coreno, M. de Simone, K. C. Prince, A. B. Trofimov, E. V. Gromo, I. L. Zaytseva and J. Schirmer, *Chem. Phys.*, 2008, **347**, 360.
8 R. S. Brown, A. Tse and J. C. Vedera, *J. Am. Chem. Soc.*, 1980, **102**, 1174.
9 I. Powis, E. E. Rennie, U. Hergenhahn, O. Kugeler and R. Bussy-Socrate, *J. Phys. Chem. A*, 2003, **107**, 25.
10 K. C. Prince, P. Bolognesi, V. Feyer, O. Plekan and L. Avaldi, *J. Electron Spectrosc. Relat. Phenom.*, 2015, **5204**, 335 and reference therein.
11 W. C. Dewey and R. M. Humphrey, *Radiat. Res.*, 1965, **26**, 538.
12 K. Sano, T. Hoshino and M. Nagai, *J. Neurosurg.*, 1968, **28**, 530.
13 T. L. P. Galvão, I. M. Rocha, M. D. M. C. Ribeiro da Silva and M. A. V. Ribeiro da Silva, *J. Phys. Chem. A*, 2013, **117**, 5826.
14 P. Bolognesi, G. Mattioli, P. O'Keeffe, V. Feyer, O. Plekan, Y. Ovcharenko, K. C. Prince, M. Coreno, A. Amore Bonapasta and L. Avaldi, *J. Phys. Chem. A*, 2009, **113**, 13593.
15 M. C. Castrovilli, P. Bolognesi, A. Cartoni, D. Catone, P. O'Keeffe, A. Casavola, S. Turchini, N. Zema and L. Avaldi, *J. Am. Soc. Mass Spectrom.*, 2014, **25**, 351.
16 P. Bolognesi, P. O'Keeffe, Y. Ovcharenko, L. Avaldi and V. Carravetta, *J. Chem. Phys.*, 2012, **136**, 154308.
17 P. Bolognesi, P. O'Keeffe, E. Ovcharenko, M. Coreno, L. Avaldi, V. Feyer, O. Plekan, K. C. Prince, W. Zhang and V. Carravetta, *J. Chem. Phys.*, 2010, **133**, 034302.
18 P. O'Keeffe, P. Bolognesi, A. Casavola, D. Catone, N. Zema, S. Turchini and L. Avaldi, *Mol. Phys.*, 2009, **107**, 2025.
19 M. C. Payne, M. P. Teter, D. C. Allan, T. A. Arias and J. D. Joannopulos, *Rev. Mod. Phys.*, 1992, **64**, 1045.
20 A. Baiardi, M. Mendolicchio, V. Barone, G. Fronzoni, G. A. Cardenas Jimenez, M. Stener, C. Grazioli, M. de Simone and M. Coreno, *J. Chem. Phys.*, 2015, **143**, 204102.
21 K. C. Prince, R. R. Blyth, R. Delaunay, M. Zitnik, J. Krempasky, J. Slezak, R. Camilloni, L. Avaldi, M. Coreno, G. Stefani, C. Furlani, M. De Simone and S. Stranges, *J. Synchotron Rad.*, 1998, **5**, 565.
22 P. Melpignano, S. Di Fonzo, A. Bianco and W. Jark, *Rev. Sci. Instrum.*, 1995, **66**, 2125.
23 M. Tronc, G. C. King and F. H. Read, *J. Phys. B: At. Mol. Phys.*, 1979, **12**, 137.
24 G. R. Wight and C. E. Brion, *J. Electron Spectrosc. Relat. Phenom.*, 1974, **3**, 191.
25 R. N. S. Sodhi and C. E. Brion, *J. Electron Spectrosc. Relat. Phenom.*, 1984, **34**, 363.
26 P. van der Straten, R. Mongerstern and A. Niehaus, *Z. Phys. D*, 1988, **8**, 35.

27 T. Hatamoto, M. Matsumoto, X.-J. Liu, K. Ueda, M. Hoshino, K. Nakagawa, T. Tanaka, H. Tanaka, M. Ehara, R. Tamaki and H. Nakatsuji, *J. Electron Spectrosc. Relat. Phenom.*, 2007, **155**, 54.
28 V. Myrseth, J. D. Bozek, E. Kukk, L. J. Saethre and T. D. Thomas, *J. Electron Spectrosc. Relat. Phenom.*, 2002, **122**, 57.
29 B. Kempgens, A. Kivimaki, M. Neeb, H. M. Köppe, A. M. Bradshaw and J. Feldhaus, *J. Phys. B: At. Mol. Phys.*, 1996, **29**, 5389; T. D. Thomas, W. Robert Jr. and J. Shaw, *J. Electron Spectrosc. Relat. Phenom.*, 1974, **5**, 1081.
30 K. C. Prince, L. Avaldi, M. Coreno, R. Camilloni and M. De Simone, *J. Phys. B: At., Mol. Opt. Phys.*, 1999, **32**, 2551.
31 P. Giannozzi, S. Baroni, N. Bonini, M. Calandra, R. Car, C. Cavazzoni, D. Ceresoli, G. L. Chiarotti, M. Cococcioni, I. Dabo, S. de Gironcoli, S. Fabris, G. Fratesi, R. Gebauer, U. Gerstmann, C. Gougoussis, A. Kokalj, M. Lazzeri, L. Martin-Samos, N. Marzari, F. Mauri, R. Mazzarello, S. Paolini, A. Pasquarello, L. Paulatto, C. Sbraccia, S. Scandolo, G. Sclauzero, A. P. Seitsonen, A. Smogunov, P. Umari and R. M. Wentzcovitch, *J. Phys.: Condens. Matter*, 2009, **21**, 395502; P. Giannozzi, O. Andreussi, T. Brumme, O. Bunau, M. Buongiorno Nardelli, M. Calandra, R. Car, C. Cavazzoni, D. Ceresoli, M. Cococcioni, N. Colonna, I. Carnimeo, A. Dal Corso, S. de Gironcoli, P. Delugas, R. A. DiStasio Jr., A. Ferretti, A. Floris, G. Fratesi, G. Fugallo, R. Gebauer, U. Gerstmann, F. Giustino, T. Gorni, J. Jia, M. Kawamura, H.-Y. Ko, A. Kokalj, E. Küçükbenli, M. Lazzeri, M. Marsili, N. Marzari, F. Mauri, N. L. Nguyen, H.-V. Nguyen, A. Otero-de-la-Roza, L. Paulatto, S. Poncé, D. Rocca, R. Sabatini, B. Santra, M. Schlipf, A. P. Seitsonen, A. Smogunov, I. Timrov, T. Thonhauser, P. Umari, N. Vast, X. Wu and S. Baroni, *J. Phys.: Condens. Matter*, 2017, **29**, 465901.
32 N. Troullier and J. L. Martins, *Phys. Rev. B: Condens. Matter Mater. Phys.*, 1991, **43**, 1993.
33 A. D. Becke, *J. Chem. Phys.*, 1993, **98**, 5648.
34 C. Lee, W. Yang and R. G. Parr, *Phys. Rev. B: Condens. Matter Mater. Phys.*, 1988, **37**, 785.
35 E. Pehlke and M. Scheffler, *Phys. Rev. Lett.*, 1993, **71**, 2338.
36 F. Rondino, D. Catone, G. Mattioli, A. Amore Bonapasta, P. Bolognesi, A. Casavola, M. Coreno, P. O'Keeffe and L. Avaldi, *RSC Adv.*, 2014, **4**, 5272.
37 G. Mattioli, F. Filippone, P. Giannozzi, R. Caminiti and A. A. Bonapasta, *Chem. Mater.*, 2009, **21**, 4555.
38 F. Neese, The ORCA program system, *Wiley Interdiscip. Rev.: Comput. Mol. Sci.*, 2012, **2**, 73.
39 F. Weigend and R. Ahlrichs, *Phys. Chem. Chem. Phys.*, 2005, **7**, 3297.
40 C. van Wüllen, *J. Chem. Phys.*, 1998, **109**, 392.
41 G. te Velde, F. M. Bickelhaupt, E. J. Baerends, C. Fonseca Guerra, S. J. A. van Gisbergen, J. G. Snijders and T. Ziegler, *J. Comput. Chem.*, 2001, **22**, 931.
42 J. P. Perdew and Y. Wang, *Phys. Rev. B: Condens. Matter Mater. Phys.*, 1986, **33**, 8800; J. P. Perdew, J. A. Chevary, S. H. Vosko, K. A. Jackson, M. R. Pederson, D. J. Sing and C. Fiolhais, *Phys. Rev. B: Condens. Matter Mater. Phys.*, 1992, **46**, 6671.
43 E. van Lenthe and E. J. Baerends, *J. Comput. Chem.*, 2003, **24**, 1142.
44 A. J. Sadlej and J. G. Snijders, *Chem. Phys. Lett.*, 1994, **229**, 435.
45 J. Zheng, X. Xu and D. G. Truhlar, *Theor. Chem. Acc.*, 2010, **128**, 295.
46 J. Kauczor, P. Norman, O. Christiansen and S. Coriani, *J. Chem. Phys.*, 2013, **138**, 124311.
47 J. Wenzel, M. Wormit and A. Dreuw, *J. Comput. Chem.*, 2014, **35**, 1900.
48 D. R. Nascimento and A. E. DePrince III, *J. Phys. Chem. Lett.*, 2017, **8**, 2951.
49 T. Yanai, D. Tew and N. Handy, *Chem. Phys. Lett.*, 2004, **393**, 51–57.
50 S. Grimme, *J. Chem. Phys.*, 2006, **124**, 034108.
51 N. A. Besley, M. J. G. Peach and D. J. Tozer, *Phys. Chem. Chem. Phys.*, 2009, **11**, 10350.
52 V. Feyer, O. Plekan, R. Richter, M. Coreno, G. Vall-llosera, K. C. Prince, A. B. Trofimov, I. L. Zaysteva, T. E. Moskovskaya, E. V. Gromov and J. Schirner, *J. Phys. Chem. A*, 2009, **113**, 5730.
53 M. Y. Choi and R. E. Miller, *J. Am. Chem. Soc.*, 2006, **128**, 7320.
54 M. Y. Choi and R. E. Miller, *J. Phys. Chem. A*, 2007, **111**, 2475.
55 V. Feyer, O. Plekan, R. Richter, M. Coreno, K. C. Prince, A. B. Trofimov, I. L. Zaysteva and J. Schirner, *J. Phys. Chem. A*, 2010, **114**, 10270.
56 F. A. Carey and R. J. Sundberg, *Advanced Organic Chemistry*, Springer, 2007.
57 K. Siegbahn, C. Nordling, A. Fahlman, R. Nordgren, K. Hamrin, J. Hedman, G. Johansson, T. Begmark, S. E. Karlsson, I. Lindgren and B. Lindberg, *ESCA Atomic,Molecular, and Solid State Structure Studied by Means of Electronic Spectroscopy*, Almqvist and Wiksell, Uppsala, 1967; K. Hamrin, G. Johansson, A. Fahlman, C. Nordling and K. Siegbahn, *Chem. Phys. Lett.*, 1968, **1**, 557.
58 T. D. Thomas, *J. Am. Chem. Soc.*, 1970, **92**, 4184.
59 A. P. Hitchcock, M. Pocock, C. E. Brion, M. S. Banna, D. C. Frost, C. A. Mcdowell and B. Wallbank, *J. Electron Spectrosc. Relat. Phenom.*, 1978, **13**, 345.
60 C. T. Chen, Y. Ma and F. Sette, *Phys. Rev. A: At., Mol., Opt. Phys.*, 1989, **40**, 6737.